Volume 9 | Number 14 | 21 July 2022

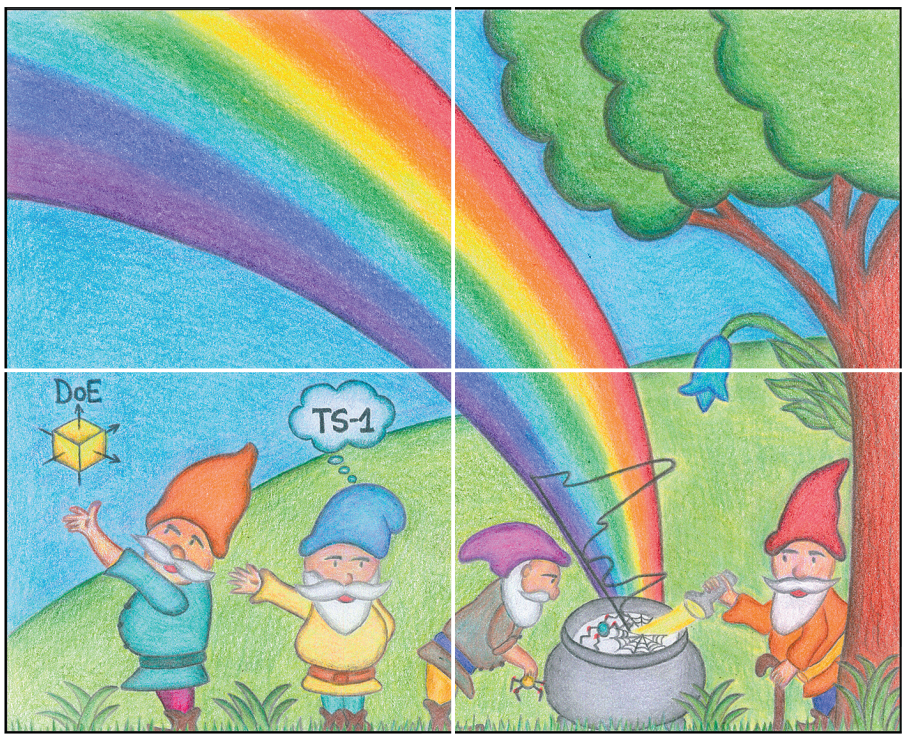

INORGANIC CHEMISTRY

FRONTIERS

CCS 中国化学会 CHINESE CHEMICAL SOCIETY
PEKING UNIVERSITY 1898
ROYAL SOCIETY OF CHEMISTRY
rsc.li/frontiers-inorganic

INORGANIC CHEMISTRY
FRONTIERS

RESEARCH ARTICLE

View Article Online
View Journal | View Issue

Cite this: *Inorg. Chem. Front.*, 2022, **9**, 3372

Rationalization of TS-1 synthesis through the design of experiments†

Francesca Rosso, Andrea Rizzetto, ‡ Alessia Airi, Khrystyna Khoma, ‡ Matteo Signorile, Valentina Crocellà, Silvia Bordiga, Simone Galliano, Claudia Barolo, Eugenio Alladio * and Francesca Bonino *

Received 28th March 2022,
Accepted 29th April 2022

DOI: 10.1039/d2qi00643j

rsc.li/frontiers-inorganic

Titanium Silicalite-1 (TS-1) is a zeolite used as a catalyst in partial oxidation reactions, whose synthesis is often performed under hydrothermal conditions by exploiting alkoxides as Ti and Si precursors. A rational study of the synthesis procedure of TS-1 using the experimental design approach was performed. Seven variables (*i.e.* times and temperatures of the various synthesis steps) were explored, by fixing the reagents ratio to establish which of them could affect the Ti incorporation and speciation. The syntheses were chosen following a D-optimal experimental design strategy, and each variable was explored at two levels and one center point. The responses monitored were: the yield of the synthesis; the total Ti content of the catalyst; the wavelength for the onset of the Ligand-to-Metal Charge Transfer (LMCT) transition involving Ti; and the vibrational fingerprint of tetrahedral Ti (centred at 960 cm^{-1} in the IR spectra). It was found that a few variables affect the Ti content and speciation (time and temperature of the hydrothermal treatment and the time of hydrolysis of the Ti precursor), whereas the yield is determined by the time of crystallization.

Introduction

Zeolites are crystalline microporous (alumino)silicates that can have both natural and synthetic origin. The most used procedure to synthesize zeolites is the hydrothermal treatment inside autoclaves or digestors, which aims at emulating the conditions occurring during their natural formation (burial metamorphic environments, saline alkaline lakes, geothermal environments, *etc.*).[1] Si- and metal-alkoxides are commonly used as the elemental source, and the synthetic procedure is usually based on three steps: (i) hydrolysis of the alkoxides; (ii) aging, possibly in the presence of an Organic Structure Directing Agent (OSDA), when the polymerization and the nucleation begin; and (iii) the hydrothermal crystallization step.[2] The conditions used in each step may affect the thermodynamics and the kinetics of the zeolite formation; therefore, many efforts were devoted to study the zeolite crystallization mechanism under hydrothermal conditions,[3–7] and particular attention was delivered to the synthesis of highly or purely siliceous materials.[8–14]

In most of the cases the optimization of the zeolite synthetic procedure is still carried on by the trial-and-error process; this procedure may sometimes lead to outstanding results, but its success is mainly based on serendipity and/or the personal experience of the synthesizer, and therefore it is complex to teach or transfer to other experimenters. Moreover, many attempts to rationalise the zeolite syntheses are done by the One-Variable-At-Time method (OVAT), which is often far from reality, especially when the system under investigation is complex as the formation of a zeolite is.

The multiple conditions adopted in each synthesis step can individually influence the final material, and the singular effects are, in most cases, hardly distinguishable. The determination of the factors affecting the synthesis of zeolites is a very challenging issue, since the investigation of the final result of the synthesis leads to the overlap of all the effects. For this purpose, many literature studies involve the interruption of the synthesis for the characterization of every step product,[15,16] but this procedure may strongly modify the material itself. The modification is unavoidable when studying the hydrothermal treatment because the step-by-step analysis implies the quenching of the autoclaves for separating the intermediate material during the crystal formation. On the contrary, the most interesting results in the study of the crystallization mechanism were obtained without isolating the intermediates

Department of Chemistry, NIS and INSTM Reference Centre, Università di Torino, Via G. Quarello 15, 10135 and Via P. Giuria 7, 10125, Torino, Italy.
E-mail: eugenio.alladio@unito.it, francesca.bonino@unito.it

†Electronic supplementary information (ESI) available. See DOI: https://doi.org/10.1039/d2qi00643j

‡Present address: Department of Applied Sciences and Technology, Politecnico di Torino, Corso Duca degli Abruzzi 24, 10129, Torino, Italy

from the autoclaves, by studying colloidal systems[17–19] and by *in situ* studies of the crystallization.[20] For this reason, the development of non-invasive and easily applicable techniques to study the zeolite synthesis and the parameters affecting their formation, avoiding the separation of intermediates, is needed.

Despite the importance of the fundamental understanding of the crystallization mechanism of zeolites, it is often difficult to correlate its results with practical indications that can be used to improve the synthetic method, and when a new catalyst has to be designed, a (semi)empirical optimization step is always required.

An approach that could overcome both these issues is the use of the Design of Experiments (DoE)[21,22] and the Multivariate Data Analysis (MDA).[23,24] The DoE is a way to plan and conduct experiments to extract the maximum amount of information from the data collected, even in the presence of noise. It can screen the influence of the experimental variables and their interactions on the result and/or optimize a procedure. The DoE approach was already used to study the synthesis of zeolites, both to explore all the frameworks that can be obtained in a broad range of conditions[25–27] and to optimize the synthesis conditions for an already discovered material, in a smaller range of variables.[28–32] Nevertheless, it was never applied to the synthesis of Titanium Silicalite-1 (TS-1), a zeolite whose preparation features many synthetic difficulties, still not unequivocally clarified, beyond the wide literature on the field.[33–43] The possibility to control and direct the speciation of Ti(IV) represents the most challenging aspect in the TS-1 synthesis and, at the same time, the most relevant feature for the catalyst, since the coordination of the Ti(IV) centres in the TS-1 framework directly influences the catalytic properties of the material. The introduction of heteroatoms in highly or purely siliceous frameworks allows obtaining functional materials with tuneable catalytic properties and, in particular, the isomorphous substitution of Si by Ti into a purely siliceous framework produces a material able to catalyse partial oxidation reactions under mild conditions, using hydrogen peroxide (H_2O_2) as the oxidizing agent.[44–50,33,34] The TS-1 was originally patented by Taramasso *et al.* in 1983. It presents the MFI framework of Silicalite-1 in which a little percentage of Ti(IV) cations partially replaces Si.[33] Afterwards, TS-1 has been successfully used at an industrial scale to produce, *e.g.*, pyrocatechol and hydroquinone from phenol and cresols from toluene.[51] Epoxidation reactions of propylene and bulkier olefines to produce epoxides were also extensively studied, both at an academic and at an industrial scale.[45–50,52–55] The applicability of TS-1 as partial oxidation catalyst is strictly dependent on the steric limitations imposed by the dimensions of the MFI pores, that imply diffusional constrictions to bulky substrates and easy deactivation of the catalyst by coke formation. The efforts devoted in trying to resolve the diffusional problems are various, some examples are the hierarchization of TS-1,[56,46,47] the production of nanosized TS-1[57,58] or the formation of hollows into bulk TS-1.[59,60] These and other attempts to modify the TS-1 for varying its catalytic properties are reported in Scheme S1.†

On the other hand, the activity of the TS-1 is determined by the nature of the active site represented by the framework Ti(IV) centres and it is affected by the not optimal Ti coordination. The activity of TS-1 in presence of H_2O_2 depends on the geometry of the interaction of the Ti(IV) site with H_2O_2. When tetrahedral Ti is involved, Ti-peroxo or Ti-hydroperoxo active species are formed upon adsorption of a H_2O_2 molecule and hydrolysis of a Ti–O–Si bond.[45,53–55] When Ti sites present distorted coordination from tetra- to octahedral, the different interaction with H_2O_2 may lead to a different catalytic cycle and the catalytic activity of these sites is hardly debated.[61,49,50] For this reason, their formation should be avoided during synthesis to improve the control over the catalytic process.

The efforts made to improve the Ti insertion and speciation are aimed at avoiding the formation of the less active bulk titanium dioxide (TiO_2). The patented TS-1 synthetic procedure involves the hydrolysis of Si and Ti alkoxides (the tetraethylorthosilicate, TEOS, and the tetraethylorthotitanate, TEOT, respectively), followed by the crystallization in an aqueous solution of tetrapropylammonium hydroxide (TPAOH) as OSDA. This synthesis should produce a zeolite in which some Si atoms are isomorphously substituted by Ti ones, in tetrahedral coordination. Nevertheless, real samples often deviate from this sharp definition, presenting Ti(IV) species at coordination different from the tetrahedral one. The commonly adopted syntheses suffer from a poor control over the correct insertion of Ti into the framework (leading to a lower and/or not optimized catalytic activity) and from a low reproducibility of the products. The critical analysis of the literature[37–44,62–64,35,36] on the topic shows that the precise influence of the Ti and Si sources and other synthetic parameters on the Ti(IV) insertion and speciation is still unclear and that no attention is usually paid on the control of accidental seeding occurring inside the Teflon liners. These parameters seem to be hardly operator dependent. The general rule about the alkoxide hydrolysis is that the hydrolysis rate of the alkoxides increases upon decreasing the length of the organic chain and the hydrolysis of the transition metals alkoxides is always faster than that of non-metallic elements, due to their electronic vacancies.[65] As a consequence, the precipitation of the more stable TiO_2 instead of the formation of the less stable tetrahedral coordinated Ti is favoured by the TEOT hydrolysis being much faster than TEOS one and by the approaching of the intrinsic incorporation limit of ≈2.7 wt% TiO_2 for tetrahedral Ti in the MFI framework.[62] To overcome, at least partially, this issue, TEOT was progressively substituted at a laboratory scale by Ti alkoxides with longer organic chains,[65] such as tetrapropylorthotitanate (TPOT) or tetrabutylorthotitanate (TBOT). Nevertheless, this strategy is insufficient to completely avoid the TiO_2 formation.[36–38] To further surmount this problem, some research focused on the use of additives, called crystallization mediating agents, coupled with the use of TBOT. Among them, it is worth mentioning: (i) H_2O_2,[39–41,66] as already suggested in the original patent,[33] which coordinates to Ti and forms water-soluble complexes, thus avoiding the precipitation of TiO_2; (ii) isopropyl alcohol

(IPA),[42,36,41] as solvent for the Ti alkoxide hydrolysis, which slows its hydrolysis and physically separates the TiO_4^{4-} hydrolysed units; and (iii) ammonium carbonate ($(NH_4)_2CO_3$),[43,35] which buffers the increasing pH during TEOS hydrolysis and favours the gelation of the solution.

In particular, the hydrolysis of TBOT in IPA is a widely used approach,[39,41,36,37] but the published results regarding Ti incorporation and speciation obtained are contrasting,[36,62–64] and it is hardly distinguishable if a specific "good result" arises from the overall synthetic procedure or the use of IPA as crystallization mediating agent. For this reason, the study with the DoE approach of the TS-1 synthesis by TBOT hydrolysis in IPA may help to shed light on the incorporation of Ti into the MFI framework with this synthetic strategy. The parameters of all the steps of the synthesis were explored, using the DoE approach and the work was supported by the MDA on the obtained results. An accurate evaluation of the reproducibility of the synthetic procedure and the control over the accidental seeding inside the liners, by hydrofluoric acid (HF) washings, was also performed.

Consequently, we present herein a rational study of the TS-1 synthesis, where the separate hydrolysis of TEOS (in the aqueous solution of the OSDA) and TBOT (in IPA at low temperature) were employed and where the times and temperatures of hydrolysis, aging and hydrothermal crystallization were explored with a D-optimal design. Besides the yield of the synthesized materials, the Ti content and speciation, using a multi-technique approach, were evaluated. These outcomes were then used as responses for the DoE,[22] fitted with the Partial Least Squares (PLS)[67] method and further explored by the Principal Component Analysis (PCA)[24] in order to identify trends and correlations among the synthetic conditions and the properties of the obtained catalysts. Moreover, significant and insignificant effects were discerned thanks to a careful evaluation of the experimental variability by repeating the same synthesis several times (for reproducibility assessment). The catalytic activity of the samples was not evaluated, since it falls out of the scope of the present work and it calls for a dedicated study. In this work, the total Ti amount was determined by Energy Dispersive X-rays spectroscopy (EDX), the tetrahedral Ti content was evaluated by the integrated area of 960 cm^{-1} signal in the infrared (IR) spectra[69,45,68] and the presence of Ti species of coordination different from the tetrahedral one was determined using the onset wavelength for the Ligand to Metal Charge Transfer (LMCT) electronic transition associated to Ti, in the ultraviolet (UV) range.[71,45,70]

Experimental

Chemicals

For the TS-1 syntheses, tetraethylorthosilicate (TEOS, reagent grade 98%, from Sigma Aldrich), tetrabutylorthotitanate (TBOT, reagent grade 97% from Sigma Aldrich), tetrapropylammonium hydroxide solution (TPAOH, 1.0 M in H_2O from Sigma Aldrich), isopropyl alcohol (IPA, ACS reagent, ≥99.8% from Sigma Aldrich) and Milli-Q water (18.2 MΩ cm^{-1}) were used. All the reagents were used without further purification.

Synthesis of TS-1 samples

Synthesis procedure. Six reproduced samples and thirteen DoE samples were prepared using a fixed stoichiometry (1 SiO_2 : 0.014 TiO_2 : 0.27 TPAOH : 2 IPA : 4 EtOH : 0.056 BuOH 40.5 H_2O) and varying the times (t) and temperatures (T) of the different steps of the synthesis.

In a typical procedure: (i) Solution A was prepared by adding 6.25 g of TEOS dropwise to 8.20 g of TPAOH diluted in 15.33 g of Milli-Q water; this solution was hydrolysed at a temperature T(H-TEOS) for a time t(H-TEOS) under reflux conditions. Solution B was prepared by adding 0.15 g of TBOT dropwise to 3.06 g of IPA and it was hydrolysed at 0 °C for a time t(H-TBOT). (ii) At the end of both the hydrolysis, solution A was cooled down to 0 °C and added dropwise to solution B under vigorous stirring; the resultant was aged at a temperature T(A) for a time t(A) under reflux conditions for gelification. (iii) The gel was crystallized at a temperature T(Cry) for a time t(Cry) in a Teflon lined stainless steel digestor of 45 ml volume, under static conditions.

At the end of the crystallization, each sample was recovered by centrifugation, washed with abundant deionized water and dried at 60 °C for 24 h. The resulting powder was then calcined in air at 550 °C for 7 h, under static conditions in a muffle furnace. After each use, the liners were washed with HF to avoid accidental seeding. Alcohols (*i.e.* ethanol (EtOH) from TEOS hydrolysis, butanol (BuOH) from TBOT hydrolysis and IPA) elimination from the synthesis mixture was avoided, since the separation by rotary evaporation resulted scarcely reproducible and did not allow for the precise control of the stoichiometry of the synthesis. Table S1† summarises the conditions used for all the synthesized samples.

Reproducibility assessment. The reproducibility of this procedure was assessed by repeating three times the same synthesis, before (Ei-a samples,) and after (Ei-b,) all the DoE set of samples, for verifying the absence of any uncontrolled variables influencing the results, such as the aging of the reagents.

D-optimal design. The DoE was used to simultaneously screen the effect of the seven variables on the Ti insertion and speciation. The samples were selected following a D-optimal design at two levels, composed of 9 syntheses (N1–N9 samples) and a centre point (N10). The syntheses N11–N13 were added to the set of DoE samples, since the conditions used are included in the experimental domain. The levels used for each variable are reported in Table 1, and the list of the syntheses and the levels used for each synthesis is reported in Table 2.

TS-1 characterization

A brief description on the methodologies used to obtain the responses adopted in DoE follows. Full details are available in the Section S2 of the ESI.†

Table 1 High (+1), intermediate (0) and low (−1) levels used for each variable

Name	+1	0	−1
t(H-TEOS)[a] (h)	24	14	4
t(H-TBOT)[b] (h)	24	14	4
T(H-TEOS)[c] (°C)	60	40	20
t(A)[d] (h)	48	36	24
T(A)[e] (°C)	60	40	20
t(Cry)[f] (h)	168	96	24
T(Cry)[g] (°C)	170	140	110

[a] t(H-TEOS): TEOS hydrolysis time. [b] t(H-TBOT): TBOT hydrolysis time. [c] T(H-TEOS): TEOS hydrolysis temperature. [d] t(A): Aging time. [e] T(A): Aging temperature. [f] t(Cry): Crystallization time. [g] T(Cry): Crystallization temperature.

Yield and crystallinity. The yield (%) of the calcined materials was used as a response for the DoE. X-Rays Diffraction (XRD) patterns were collected on the as-synthesized samples with a Cu Kα radiation on a PANalytical X'Pert diffractometer (Bragg-Brentano geometry), in the range $5° \leq 2\theta \leq 50°$, with a step of 0.02° and 50 s of integration per step.

Ti characterization. The total Ti content (defined as "Ti/Si × 100") was determined by an EDX detector (Oxford – Detector with an AZTEC software) set on a Field Emission Scanning Electron Microscope (Tescan S9000G with a Scottky FEG source) and it was used as a response for the DoE.

The speciation of Ti was assessed using UV spectroscopy in Diffuse Reflectance (DR) mode and Fourier Transform (FT) IR spectroscopy in Attenuated Total Reflectance (ATR) mode. DR-UV spectra were collected on a Varian Cary5000 spectrophotometer, equipped with a DR sphere, on the pure samples (Spectralon® was used as 100% reflectance reference). All the samples were measured as such and after the following activation procedure, aiming at eliminating the influence of water on the Ti coordination, as well as that from possible organic pollutants: the samples were heated to 500 °C with a ramp of 5° per min under dynamic vacuum (residual pressure < 10^{-3} mbar), outgassed for 1 h at 500 °C and then exposed to 100 mbar of pure oxygen (O_2) for 30 min; the samples were finally further outgassed for 1 h prior cooling.[45] After the activation, the samples were transferred from the activation cell to the measurement holder inside a glovebox (H_2O < 0.5 ppm), in order to avoid any rehydration or contamination. The onset wavelength for the LMCT electronic transitions involving Ti (hereafter "LMCT onset"), was used as a response for the DoE (calculated as shown in Fig. S1†), as indication of the presence of non-tetrahedral Ti species; in detail, an LMCT onset value larger than 335 nm (Fig. S2†) is representative for the presence of Ti species with a coordination number higher than for the perfect tetrahedral sites (*i.e.* > 4). ATR-IR spectra were recorded on a Bruker Alpha II spectrophotometer located inside the glovebox, on the same samples pre-activated for the sake of DR-UV measurements. The spectra were recorded with a DTGS detector by accumulating 32 scans (64 for the background spectrum), with a resolution of 2 cm^{-1}. The integrated area of the 960 cm^{-1} signal (hereafter "960 cm^{-1} area"), quantitatively correlated to the amount of tetrahedrally coordinated Ti inserted in the MFI framework,[45,68] was used as a response for the DoE.

Analysis of data. The MDA was performed with the PLS regression[67] using the MODDE® 13 software by Sartorius Stedim Data Analytics.[72] The chosen D-optimal design allows the determination of only linear terms so that, for each response, a straight line in the following form was obtained (eqn (1))

$$y = C + a_1x_1 + a_2x_2 + a_3x_3 + a_4x_4 + a_5x_5 + a_6x_6 + a_7x_7 \quad (1)$$

where y is the response, x_n are the levels centred and scaled for the seven variables n (high: + 1; intermediate: 0; low: −1), C is the constant term (intercept), and a_n are the coefficients of the model, centred and scaled. When the coefficients are centred and scaled, their value is proportional to the positive or negative effect that a given variable n has on the response y, thus

Table 2 List of the syntheses and levels (high: +1; intermediate: 0; low: −1) used for each variable. Lines N1–N9: experimental matrix of the D-optimal design. Line N10: centre point. Lines N11–N13: additional syntheses in the experimental domain, included in the model. Line E: reproducibility samples

Name	t(H-TEOS)[a]	t(H-TBOT)[b]	T(H-TEOS)[c]	t(A)[d]	T(A)[e]	t(Cry)[f]	T(Cry)[g]
N1	−1	+1	−1	−1	−1	−1	−1
N2	+1	+1	+1	+1	+1	−1	−1
N3	+1	−1	+1	−1	−1	+1	−1
N4	−1	−1	−1	+1	+1	+1	−1
N5	−1	−1	+1	+1	−1	−1	+1
N6	+1	−1	−1	−1	+1	−1	+1
N7	−1	+1	−1	+1	+1	−1	+1
N8	+1	+1	−1	+1	−1	+1	+1
N9	−1	+1	+1	−1	+1	+1	+1
N10	0	0	0	0	0	0	0
N11	−1	−1	−1	+1	−1	+1	−1
N12	+1	+1	+1	+1	+1	+1	−1
N13	−1	+1	0	+1	0	−1	+1
E[h]	−1	−1	0	−1	0	−1	0

[a] t(H-TEOS): TEOS hydrolysis time. [b] t(H-TBOT): TBOT hydrolysis time. [c] T(H-TEOS): TEOS hydrolysis temperature. [d] t(A): Aging time. [e] T(A): Aging temperature. [f] t(Cry): Crystallization time. [g] T(Cry): Crystallization temperature. [h] Level used to synthesize 6 samples.

allow the comparison among the effect of different variables n. The error bar (calculated at 90% of confidence) of the coefficients can be used to determine the significance of each term in the eqn (1). The coefficients can consequently be used to identify which variable n has a significant influence on the response y, and if the effect is positive or negative (*i.e.*, if the increase of the variable causes an increase or a decrease in the response, respectively). The PLS regression was performed by including the responses of samples from N1 to N13 and the series Ei-b.

Subsequently, R software (version 4.0.2)[73] was employed to compute PCA models on datasets involving DR-UV and ATR-IR measurements (in the 200–350 nm and 1000–900 cm^{-1} ranges, respectively). The data were pre-processed by using the Standard Normal Variate (SNV) algorithm before calculating models.[74] The PCA models were used to evaluate the correlation among the responses LMCT onset and 960 cm^{-1} area with the actual variability among DR-UV and ATR-IR spectra, and to individuate correlations among the responses.

Results and discussion

TS-1 samples characterization

The experimental variability was evaluated, and the results are reported in Section S3 of the ESI.† The repeated syntheses were judge sufficiently coherent to allow the DoE approach to study the Ti insertion (Table S2 and Fig. S3†). Moreover, the comparison between the Ei-a and Ei-b series is necessary to exclude the presence of uncontrolled, variable in time parameters, that could influence the result of the syntheses (such as the aging of reagents or the adsorption of organic pollutant on the Teflon liners): such effects were eventually excluded.

Fig. 1 shows the XRD patterns (panel a), ATR-IR spectra (panel b) and DR-UV spectra (panel c) of the DoE set of samples. All the samples are highly crystalline as testified by their XRD patterns, synthesized with yields between 67% and 95% (Table 3).

Regarding the Ti speciation of the DoE set of samples, the Ti/Si × 100 is comprised between 0.59 of N3 and 1.85 of N12 (Table 3). The ATR-IR spectra of all the samples (Fig. 1b) show the typical signals of silicate materials, such as the asymmetric and symmetric Si–O–Si stretching (bands centred at ≈1100 cm^{-1} and 800 cm^{-1}, respectively) and the pentasil unit collective modes of MFI structure, peaked at 550 cm^{-1}.[75] The band centred at 960 cm^{-1} is assigned to the antisymmetric Ti–O–Si vibrations, caused by the insertion of Ti in a tetrahedral framework position.[69,45,68] The signal is visible in all the reported spectra. The integrated areas of the band at 960 cm^{-1} for each sample spectrum are listed in Table 3, and represent a quantitative indicator of the tetrahedral Ti incorporated in the MFI framework.[69,45,68]

The DR-UV spectrum of each sample (Fig. 1c) presents the LMCT electronic transition involving Ti. When only tetrahedral Ti is present in the sample, this band is peaked at approximately 200 nm and consists of a monodispersed signal (LMCT

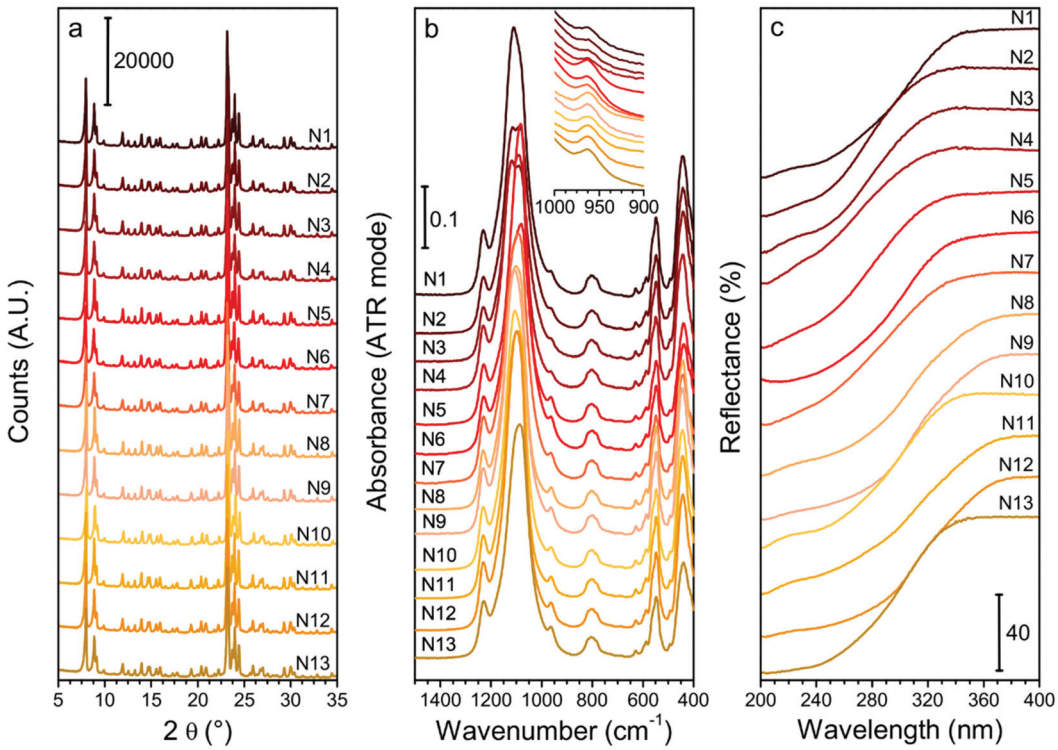

Fig. 1 (a) XRD patterns of the as synthesized full set of DoE samples; (b) ATR-IR spectra of the activated DoE samples; the inset reports the magnification of 960 cm^{-1} signal. (c) DR-UV spectra of the activated DoE samples.

Table 3 List of the responses obtained for each synthesis. Lines N1–N9: syntheses belonging to the D-optimal design. Line N10: centre point. Lines N11–N13: additional syntheses in the experimental domain, included in the model

Name	Yield (%)	Ti/Si × 100 (mol/mol)	LMCT onset (nm)	960 cm^{-1} area (cm^{-1})
N1	75.32	1.22	341	0.157
N2	73.03	0.73	314	0.122
N3	74.88	0.59	312	0.104
N4	67.53	0.69	309	0.114
N5	79.71	1.17	332	0.313
N6	69.22	1.68	353	0.298
N7	66.82	1.20	341	0.265
N8	90.58	1.79	368	0.345
N9	94.94	1.66	365	0.336
N10	74.27	1.31	335	0.286
N11	89.66	1.48	367	0.315
N12	94.82	1.85	370	0.352
N13	78.46	1.71	337	0.334

onset at about 335 nm, see Fig. S2†). The signal does not present shoulders when all the Ti is tetrahedrally coordinated. Conversely, it shifts downward and broadens progressively when intermediate pentacoordinated or hexacoordinated TiO_x species are present, or upon increasing the nuclearity of Ti centre (from isolated to multimeric centres), until reaching the wavelength of the octahedral Ti in bulk TiO_2 (peaked at ≈320 nm, with an LMCT onset at 380 nm, Fig. S2†).[76,45,70] When intermediate defective sites among the bulk TiO_2 and the tetrahedral Ti are present, additional components peaked between 260–280 nm arises[45,76] (with onset around 360 nm in the case octahedral species are the dominant class of defects, Fig. S2†). However, the relative intensity of those components cannot be used for a quantitative purpose since the extinction coefficient for each component is unknown.[45] For these reasons, in this work, the intermediate Ti sites were not quantified, but their presence was qualitatively evaluated using the wavelength at which the LMCT signal starts (LMCT onset in Table 3). All the samples present the spectral component due to tetrahedral Ti (accordingly to the presence of the 960 cm^{-1} signal in the IR range of frequencies), and none of them presents the component assigned to bulk TiO_2. This result implies that the slow hydrolysis of TBOT at 0 °C in IPA is effective in avoiding the TiO_2 formation in the whole experimental domain. The presence of intermediate non-tetrahedral Ti species is testified in the majority of the samples by the LMCT band broadening and, occasionally, by the presence of defined shoulders, highlighting distinct additional maxima (*e.g.*, in the samples N3 and N9).

Analysis of the responses through the DoE

The effect of each variable (listed in the Synthesis procedure section) on the yield of the synthesis, the Ti/Si × 100 or the Ti speciation (LMCT onset and 960 cm^{-1} area) was screened with a limited number of experiments (19 synthesis including both the DoE and the reproducibility samples). For each response, the positive or negative linear effect of each variable was calculated, as expressed by the coefficient plots in Fig. 2.

The coefficient plot shows a column reporting the average value of the response (constant term) obtained with the synthesis procedure and other columns reporting the effects of the synthesis variables. The constant term was obtained by the intercept of eqn (1) and the other columns correspond to terms a_n of the same equation. Therefore, the columns of the synthesis variables show the margin of improvement of the response into the experimental domain upon changing the variable, to add (if positive) or subtract (if negative) to the constant term. The significant and insignificant terms can be discerned by evaluating the error bars of the columns: an effect is insignificant negligible when its error bar overpasses the zero level (*i.e.* when it is not sure if the effect is positive or negative). For this reason, Fig. 2 shows the coefficient plots for each response, before (main plot) and after (inset) the exclusion of insignificant terms. As it can be seen, the variables significantly influencing the responses are few. This outcome implies the possibility of excluding all the insignificant variables in the investigated experimental domain from further studies.

The yield coefficient plot analysis (Fig. 2a) shows that the yield of the synthesis depends only on t(Cry). The predicted confidence interval for the response are reported in Tables S3 and S4.† This result highlights how, with this synthetic procedure, the TEOS hydrolysis conditions (which supply the SiO_2 units, that give the major contribution to the yield) do not significantly affect the yield. Consequently, the yield is determined during the hydrothermal crystallization step, possibly by the equilibrium among precipitation and solubilization of silicate species, even if we do not know if the TEOS hydrolysis is quantitative during the hydrolysis step.

The Ti/Si × 100 coefficient plot analysis (Fig. 2b) indicates that the Ti/Si × 100 is significantly affected by t(H-TBOT) and T(Cry). This suggests that at 0 °C, in 4 h (the low level) the TBOT hydrolysis is not completed; therefore, the number of available TiO_4^{4-} units in SiO_4^{4-} units medium affects the Ti incorporation. Conversely, t(H-TEOS) and T(H-TEOS) do not affect Ti/Si × 100. We can deduce that the hydrolysis degree of TEOS, when it contacts the TiO_4^{4-} units, is sufficient to start and support the co-polymerization during the aging step. The insignificance of t(A) and T(A) indicates that the rate of polymerization of the SiO_4^{4-} units and the nucleation of the MFI framework (possibly influenced by t(A) and T(A)) does not significantly affect Ti/Si × 100 when the same hydrolysis conditions and T(Cry) are used. Moreover, the significant effect of T(Cry) on Ti/Si × 100 can be explained considering the common theory for which the crystal growth of the highly siliceous MFI framework occurs by addition of solubilized units from the liquid phase, when alkoxides are used as starting materials.[77,78] Therefore, the increasing of T(Cry) facilitates the incorporation of TiO_4^{4-} units from the liquid phase into the growing crystals, thus influencing the final Ti/Si × 100.

The LMCT onset coefficient plot (Fig. 2c) demonstrates as the LMCT onset is significantly affected by t(Cry) and T(Cry),

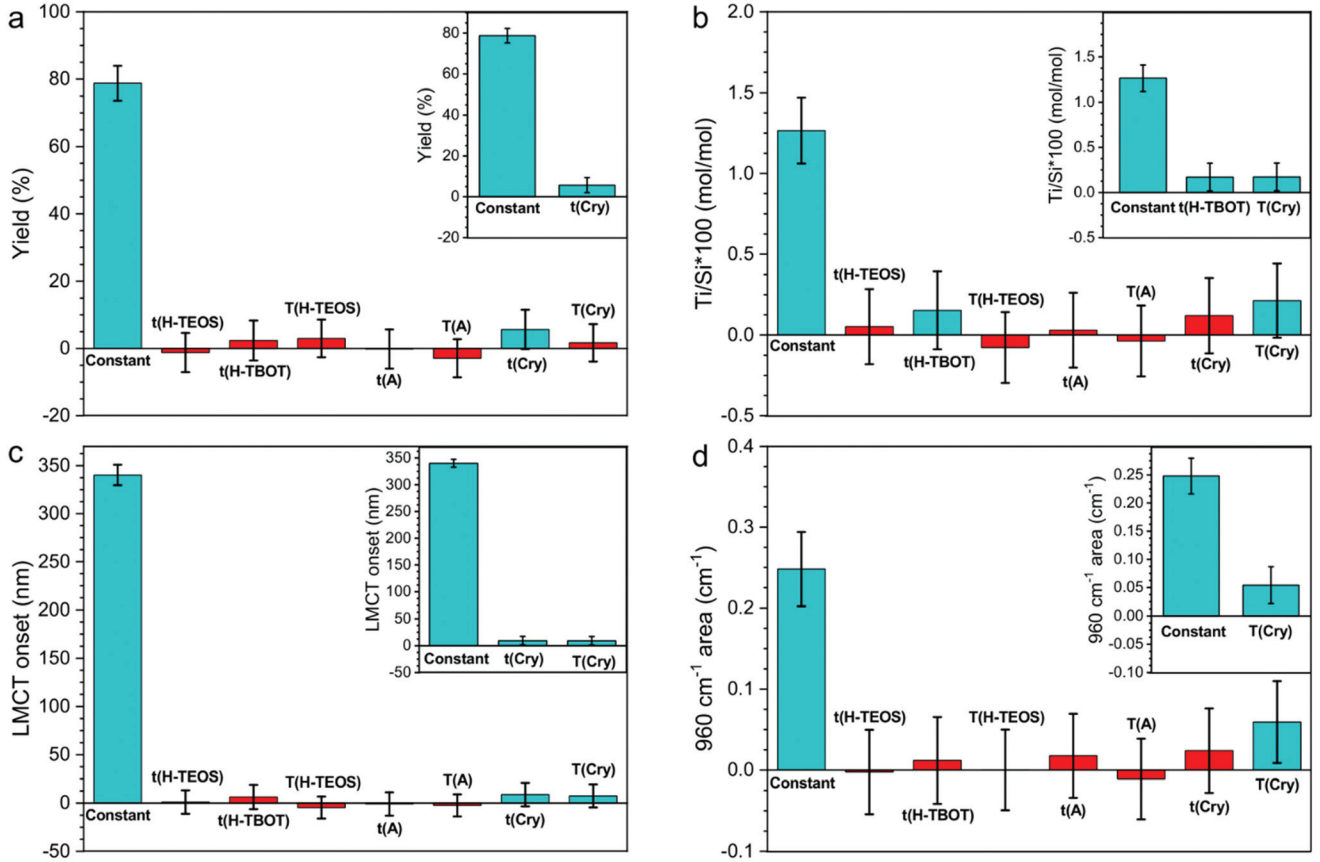

Fig. 2 Coefficient plot for each response: (a) Yield (%), (b) Ti/Si × 100 (mol mol^{-1}), (c) LMCT onset (nm) and (d) 960 cm^{-1} area (cm^{-1}). For each panel, the main plot shows the coefficient of all the variables with their error bars and the inset shows only the coefficients that have a significant influence on the response, with their error bars. For clarity, the insignificant effect columns were coloured in red and the significant effect columns were coloured in light blue.

even if their effect is small (as shown in Table S3 and S4†). This observation is coherent with the onset of the LMCT transition of the experimental DR-UV spectra (Fig. 1c and Fig. S3†), that moderately varies in the range 309–370 nm (Table 3). This result suggests that the Ti speciation is therefore influenced mainly by the synthesis procedure with slight modifications occurring during the crystal growth.

The 960 cm^{-1} area coefficient plot analysis (Fig. 2d) shows as the band's area, proportional to the concentration of the tetrahedrally coordinated Ti, is the response that more strongly varies into the experimental domain, as it can be seen by the ratio between the column of the significant variable and the column of the constant term in Fig. 2d. The variable significantly affecting the 960 cm^{-1} area is T(Cry), in accordance with the fact that the same variable affects the LMCT onset response. Considering the synthesis procedure and experimental domain chosen for this work, the marked increase of the 960 cm^{-1} area is associated to the increase of total Ti content. Since the Ti/Si × 100 experimentally obtained are all far under the theorical limit, it is plausible that an increase in the Ti/Si × 100 will proportionally lead to a rise of the tetrahedral Ti content, therefore of the 960 cm^{-1} area. Moreover, T(Cry) has also the effect of increasing the LMCT onset, *i.e.*, to increase the content of non-tetrahedral species. From these observations, it can be excluded that the increase in the temperature of crystallization might cause the transformation of non-tetrahedral Ti sites to tetrahedral ones, thus it is more reasonable to assume that the Ti is directly incorporated in the tetrahedral centres.

The general deduction is that using the synthetic procedure descripted and, within this experimental domain, the Ti/Si × 100 could be controlled, and the inserted Ti will be principally tetrahedral, but it is not possible entirely excluding the formation of non-tetrahedral species. Instead, the formation of bulk TiO_2 is totally avoided.

The contour plots (Fig. 3) show in a graphical way the effect of the significant variables (reported on the axes) and the desired direction to follow for improving the synthesis results (indicated by the warm colours). The graph in Fig. 3 reports the responses regarding Ti (Ti/Si × 100: Fig. 3a and b, LMCT: Fig. 3c, 960 cm^{-1} area: Fig. 3d). The comparison among panels b, c and d (expressed *versus* the same variable) evidenced how, with this synthesis procedure and within this experimental domain, the Ti/Si × 100 and Ti speciation (LMCT onset and

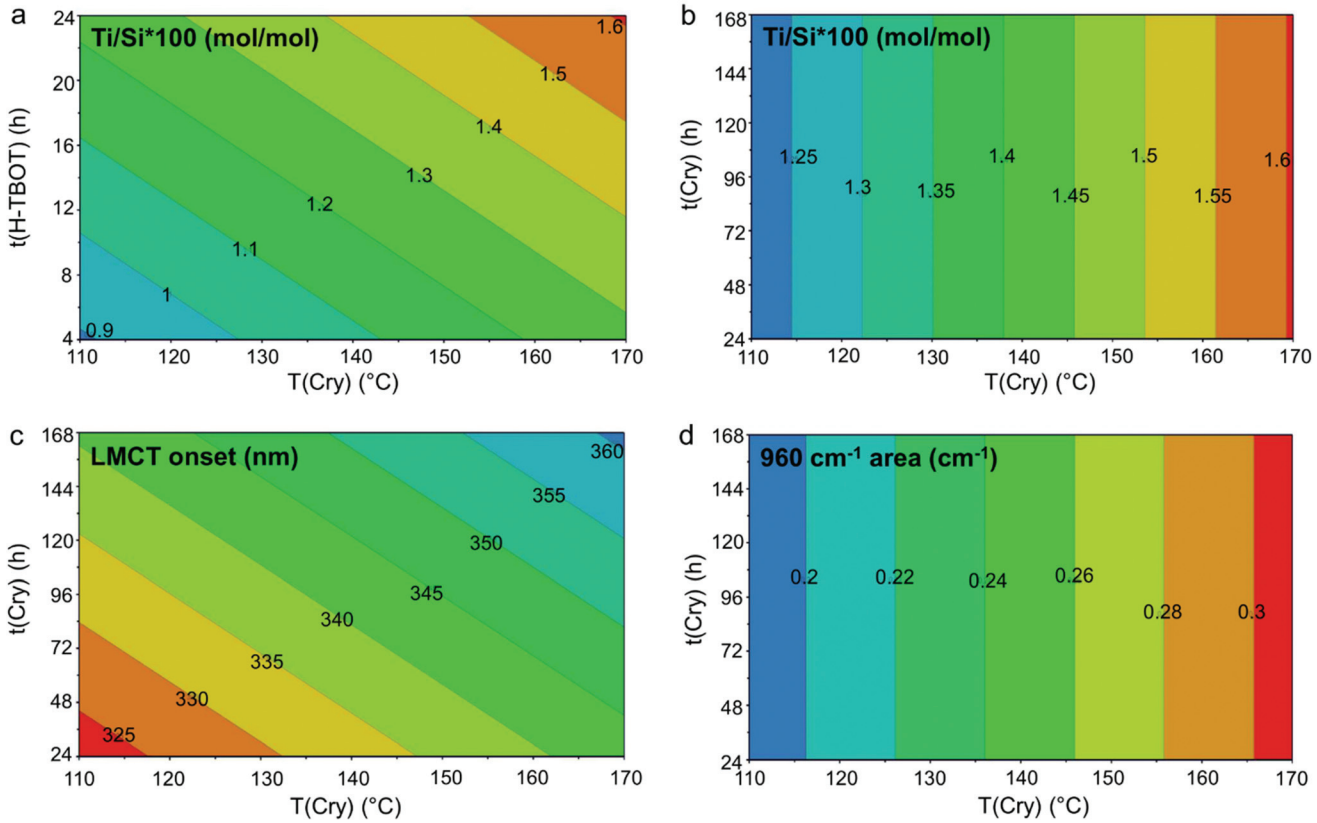

Fig. 3 Contour plots for the responses regarding Ti content (Ti/Si × 100 in panels a and b) and speciation (LMCT onset in panel c and 960 cm^{-1} area in panel d). Panels a and c report the contour plots involving the significant variables for the responses Ti/Si × 100 and LMCT onset, while panels b is included to compare the total Ti content with the LMCT onset and the 960 cm^{-1} area varying the same variables (time and temperature of crystallization). The askew bands are iso-response regions, delimited by lines which corresponding response is reported in the labels (the label have the dimension of the response).

960 cm^{-1} area) can be simultaneously improved until a specific limit, with the compromise of a fraction of Ti unavoidably incorporated as non-tetrahedral.

Finally, a digression is worth regarding the choice not to evaporate the alcohols from the synthesis mixture to favour the reproducibility of the synthesis procedure and facilitates the use of the DoE approach. Indeed, DoE requires as precise as possible knowledge of the synthesis parameters, in order to avoid the attribution to explored variables of response variations instead ascribable to uncontrolled parameters. For this reason, the evaporation of alcohols has been avoided. However, it must be considered that the addition of alcohols to hydrolysed solutions of TEOS is reported to favour the immediate polymerization and precipitation of silicate species.[79,17,63] The precipitation could have influenced the overall Ti/Si × 100 as this response is affected by the t(H-TBOT) (Fig. 2b). The t(H-TBOT) determines the number of TiO_4^{4-} units present in the TBOT/IPA solution when the TEOS/TPAOH/H_2O solution was added. The already hydrolysed TiO_4^{4-} units will probably be easily incorporated into the polymerised silicate framework, without leaving further time for the TBOT hydrolysis.

PCA of ATR-FT-IR and DR-UV data

Finally, the developed PCA models on ATR-IR and DR-UV measurements showed clear trends in the data, since they correlate with Ti/Si × 100. Fig. 4 and 5 show the PCA scores and loadings plots from the 2nd and 3rd components of the PCA models developed on ATR-IR and DR-UV data, respectively. In particular, panels 4a and 5a show the scores plots as obtained from the model, panels 4b and 5b show the same plots, where the colours of the sample spots were scaled according to the Ti/Si × 100, and panels 4c and 5c reports the loadings plots. PCA scores plots (Fig. 4 and 5, a-b) show PC2 and PC3 values since PC1, mostly representative for the overall spectral shape, did not turn to be informative when looking at the measurements monitored in the study. On the other hand, Ti/Si × 100 variability (as well as LMCT onset and the area of the 960 cm^{-1} signal, showed in Fig. S4 and S5 of the ESI†) is mainly represented by PC2 for the ATR-IR data and by PC2 and PC3 by the DR-UV data. In both the cases, the PCA scores plots showed that the samples N8, N9, N11 and N12 provided the highest values of Ti/Si × 100, in correlation with the intensity of the signal within the 950–975 cm^{-1} range for ATR-IR

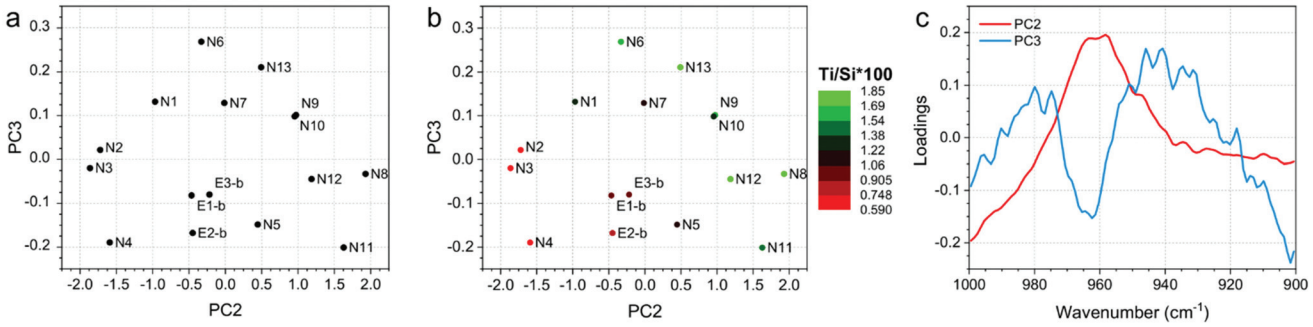

Fig. 4 (a) PC2 and PC3 scores plot, (b) PC2 and PC3 scores plot, in which the sample spots were scaled according to the Ti/Si × 100 and (c) loadings plot of the PCA model developed on ATR-IR data.

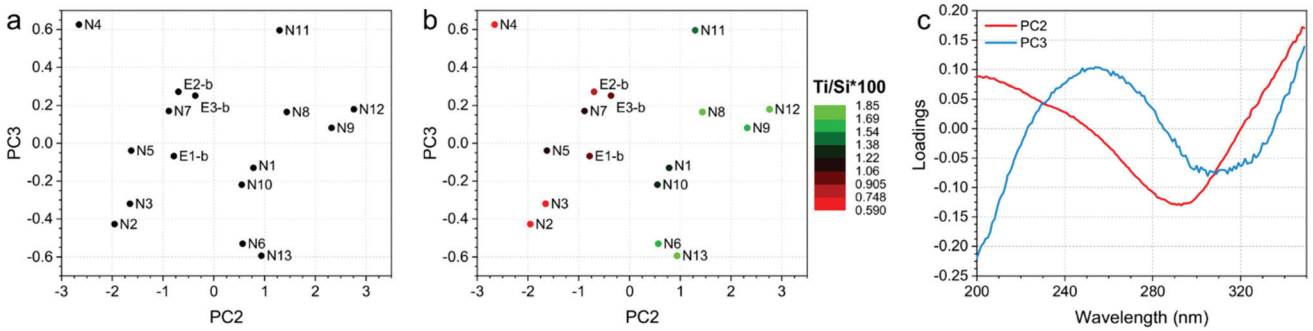

Fig. 5 (a) PC2 and PC3 scores plot, (b) PC2 and PC3 scores plot, in which the sample spots were scaled according to the Ti/Si × 100 and (c) loadings plots of the PCA model developed on DR-UV data.

measurements, and the 250–300 nm range for DR-UV measurements. These results further confirm that the increase of Ti/Si × 100 is correlated with the insertion of tetrahedrally coordinated Ti (PCA on ATR-IR data). Conversely, the content of non-tetrahedral species will also increase by raising the value of Ti/Si × 100, as can be seen by the PC2 of DR-UV data in the 250–300 nm range. The PCA analysis of ATR-IR and DR-UV spectra thus fully supports the evidences from DoE as previously commented.

Conclusions

The rational study of the synthesis of TS-1 zeolite using the DoE approach was reported to discern the synthesis parameters that significantly impact the catalyst properties. It was established that the Ti insertion and speciation is mainly determined during the hydrothermal step of the synthesis. In particular, the total Ti content (Ti/Si × 100) is increased by the time of hydrolysis of the Ti source (t(H-TBOT)) and by higher temperatures of crystallization (T(Cry)). On the other hand, Ti speciation can be controlled by varying the time of crystallization (t(Cry)) and the temperature of crystallization (T(Cry)). Regarding the variability of the responses in the explored experimental domain, the total Ti content and the area of the 960 cm^{-1} band (correlated to the concentration of the tetrahedral Ti) are determined in a certain amount by the procedure itself, but they can be heavily modified by regulating the variables. On the other hand, the LMCT onset is basically determined by the synthesis procedure and it can only be modified slightly by these variables in the experimental domain. This framework is entirely in agreement with the independent PCA analysis of the spectroscopic results.

Although the presented DoE project does not lead to the synthesis of a TS-1 sample with an elevated quantity of Ti, entirely inserted in tetrahedral framework position, this work allowed investigating the direct correlation of the synthesis variables with the results, net of the experimental variability of the procedure, using a limited number of experiments and resources. In a more general conception, DoE is a practical approach that helps identifying the issues of the procedure and their causes, leading to an exceptional improvement in the knowledge on this vast field, impossible to reach with the trial-and-error or with the OVAT approaches.

The application of this work methodology to the optimization of the present synthesis, by excluding the insignificant variables and by adding other parameters (such as different precursors or varying composition of the synthesis gel), could lead to the preparation of a "perfect" TS-1 sample, featuring Ti in the only tetrahedral positions with a concentration reaching

the theoretical insertion limit. Moreover, the same approach could be applied, in the future, to the study of Ti insertion into different zeolitic frameworks and to disclose the relation of Ti speciation with catalytic performances in partial oxidation reactions.

Author contributions

All the authors contributed in the conceptualization of the project. Francesca Rosso contributed to conceptualization, formal analysis, investigation, methodology, validation, visualization, writing – original draft. Andrea Rizzetto contributed to formal analysis, investigation, validation, visualization, writing -review and editing. Alessia Airi contributed to conceptualization, investigation, supervision, writing -review and editing. Khrystyna Khoma contributed to investigation, writing -review and editing. Matteo Signorile contributed to conceptualization, supervision, writing -review and editing. Valentina Crocellà contributed to conceptualization, supervision, writing -review and editing. Silvia Bordiga contributed to conceptualization, funding acquisition, resources, writing -review and editing. Simone Galliano contributed to conceptualization, formal analysis, methodology, validation, writing -review and editing. Claudia Barolo contributed to conceptualization, supervision, writing -review and editing. Eugenio Alladio contributed to conceptualization, formal analysis, methodology, supervision, validation, writing – original draft. Francesca Bonino contributed to conceptualization, funding acquisition, project administration, resources, supervision, writing -review and editing.

Conflicts of interest

There are no conflicts to declare.

Notes and references

1 I. Marantos, G. G. Christidis and M. Ulmanu, in *Handbook of Natural Zeolites*, ed. V. J. Inglezakis and A. A. Zorpas, Bentham E Books, 2012, pp. 28–51.
2 *Handbook of Zeolite Science and Technology*, ed. S. M. Auerchach, K. A. Carrado and P. K. Dutta, Marcel Dekker, Inc., New York, 2003.
3 S. I. Zones and Y. Nakagawa, Use of Modified Zeolites as Reagents Influencing Nucleation in Zeolite Synthesis, *Stud. Surf. Sci. Catal.*, 1995, **97**, 45–52.
4 S. Mintova, N. H. Olson, V. Valtchev and T. Bein, Mechanism of Zeolite A Nanocrystal Growth from Colloids at Room Temperature, *Science*, 1999, **283**, 958–960.
5 P. S. Singh, Complexity of silicate/aluminosilicate polymerization: some insights using a small-angle X-ray scattering study, *J. Appl. Crystallogr.*, 2007, **40**, 590–593.
6 A. Deneyer, Q. Ke, J. Devos and M. Dusselier, Zeolite Synthesis Under Nonconventional Conditions: Reagents, Reactors, and *Modi Operandi*, *Chem. Mater.*, 2020, **32**, 4884–4919.
7 A. Corma and M. E. Davis, Issues in the Synthesis of Crystalline Molecular Sieves: Towards the Crystallization of Low Framework Density Structures, *ChemPhysChem*, 2004, **5**, 304–313.
8 S. L. Burkett and M. E. Davis, Mechanism of Structure Direction in the Synthesis of Si-ZSM-5: an Investigation by Intermolecular ^{1}H ^{29}Si CP MAS NMR, *J. Phys. Chem.*, 1994, **98**, 4647–4653.
9 S. L. Burkett and M. E. Davis, Mechanism of Structure Direction in the Synthesis of Pure-Silica Zeolites. 2. Hydrophobic Hydration and Structural Specificity, *Chem. Mater.*, 1995, **7**, 920–928.
10 M. A. Camblor, A. Corma, M. J. Díaz-Cabañas and C. Baerlocher, Synthesis and Structural Characterization of MWW Type Zeolite ITQ-1, the Pure Silica Analog of MCM-22 and SSZ-25, *J. Phys. Chem. B*, 1998, **102**, 44–51.
11 C. S. Cundy, J. O. Forrest and R. J. Plaisted, Some observations on the preparation and properties of colloidal silicalites. Part I: Synthesis of colloidal silicalite-1 and titanosilicalite-1 (TS-1), *Microporous Mesoporous Mater.*, 2003, **66**, 143–156.
12 Á. Cantín, A. Corma, M. J. Díaz-Cabañas, J. L. Jordá, M. Moliner and F. Rey, Synthesis and Characterization of the All-Silica Pure Polymorph C and and Enriched Polymorph B Intergrowth of Zeolite Beta, *Angew. Chem., Int. Ed.*, 2006, **45**, 8013–8015.
13 J. Grand, H. Awala and S. Mintova, Mechanism of zeolite crystal growth: new findings and open questions, *CrystEngComm*, 2016, **18**, 650–664.
14 R. Bai, Y. Song, R. Bai and J. Yu, Creation of Hierarchical Titanosilicate TS-1 Zeolite, *Adv. Mater. Interfaces*, 2021, **8**, 2001095–2001095.
15 R. J. Francis and D. O. Hare, The kinetics and mechanism of the crystallization of microporous materials, *J. Chem. Soc. Trans.*, 1998, 3133–3148.
16 F. Fengtao, F. Zhaochi and L. Can, UV Raman spectroscopic study on the synthesis mechanism and assembly of molecular sieves, *Chem. Soc. Rev.*, 2010, **39**, 4794–4801.
17 G. Zhang, J. Sterte and B. J. Schoeman, Discrete Colloidal Crystals of Titanium Silicalite-1, *J. Chem. Soc., Chem. Commun.*, 1995, 2259–2260.
18 G. Zhang, J. Sterte and B. J. Schoeman, Preparation of Colloidal Suspensions of Discrete TS-1 Crystals, *Chem. Mater.*, 1997, **9**, 210–217.
19 A. Aerts, C. E. A. Kirschhock and J. A. Martens, Methods for *in situ* spectroscopic probing of the synthesis of a zeolite, *Chem. Soc. Rev.*, 2010, **39**, 4626–4642.
20 D. Grandjean, A. M. Beale, A. V. Petukhov and B. M. Weckhuysen, Unraveling the Crystallization Mechanism of CoAPO-5 Molecular Sieves Under Hydrothermal Conditions, *J. Am. Chem. Soc.*, 2005, **127**, 14454–14465.
21 T. Lundstedt, E. Seifert, L. Abramo, B. Thelin, A. Nystrom, J. Pettersen and R. Bergman, Experimental design and optimization, *Chemom. Intell. Lab. Syst.*, 1998, **42**, 3–40.

22 R. Leardi, Experimental Design in Chemistry: A Tutorial, *Anal. Chim. Acta*, 2009, **652**, 161–172.
23 K. Héberger, Chemoinformatics – multivariate mathematical-statistical methods for data evaluation, in *Medical Applications of Mass Spectrometry*, ed. K. Vekey, A. Telekes and A. Vertes, Elsevier B.V., 2008, pp. 141–169.
24 R. Bro and A. K. Smilde, Principal component analysis, *Anal. Methods*, 2014, **6**, 2812–2831.
25 A. Corma, M. J. Díaz-Cabanas, M. Moliner and C. Martínez, Discovery of a new catalytically active and selective zeolite (ITQ-30) by high-throughput synthesis techniques, *J. Catal.*, 2006, **241**, 312–318.
26 M. Moliner, M. J. Díaz-Cabañas, V. Fornés, C. Martínez and A. Corma, Synthesis methodology, stability, acidity and catalytic behavior of the 18 × 10 member ring pores ITQ-33 zeolite, *J. Catal.*, 2008, **254**, 101–109.
27 Z. Liu, A. Chokkalingam, S. Miyagi, M. Yoshioka, T. Ishikawa, H. Yamada, K. Ohara, N. Tsunoji, Y. Naraki, T. Sano, T. Okubo and T. Wakihara, Revealing scenarios of interzeolite conversion from FAU to AEI through the variation of starting materials, *Phys. Chem. Chem. Phys.*, 2022, **24**, 4136–4146.
28 A. De Lucas, L. Rodríguez and P. Sánchez, Optimization of the Molar Composition of the Gel in the Synthesis of Titanium Silicalite-2 TS-2, *Chem. Eng. Res. Des.*, 2000, **78**, 136–144.
29 M. Tagliabue, L. C. Carluccio, D. Ghisletti and C. Perego, Multivariate approach to zeolite synthesis, *Catal. Today*, 2003, **81**, 405–412.
30 M. Balbaşi, Application of full factorial design method to silicalite synthesis, *Mater. Res. Bull.*, 2013, **48**, 2908–2914.
31 N. Martín, M. Moliner and A. Corma, High yield synthesis of high-silica chabazite by combining the role of zeolite precursors and tetraethylammonium: SCR of NO_X, *Chem. Commun.*, 2015, **51**, 9965–9968.
32 C. F. Imbachi-Gamba and A. L. Villa, Statistical analisys of the influence of the synthesis conditions on the properties of hierarchical zeolite Y, *Mater. Today Chem.*, 2021, **20**, 100442.
33 M. Taramasso, G. Perego and B. Notari, *US Pat*, 4410501, 1983.
34 J. Přech, Catalytic performance of advanced titanosilicate selective oxidation catalysts - a review, *Catal. Rev. – Sci. Eng.*, 2018, **60**, 71–131.
35 W. Fan, B. Fan, X. Shen, J. Li, P. Wu, Y. Kubota and T. Tatsumi, Effect of ammonium salts on the synthesis and catlytic properties of TS-1, *Microporous Mesoporous Mater.*, 2009, **122**, 301–308.
36 A. Thangaraj and S. Sivasanker, An Improved Method for TS-1 Synthesis: ^{29}Si NMR Studies, *J. Chem. Soc., Chem. Commun.*, 1992, **20**, 123–124.
37 D. Lin, Q. Zhang, Z. Qin, Q. Li, X. Feng, Z. Song, Z. Cai, Y. Liu, X. Chen, D. Chen, S. Mintova and C. Yang, Reversing Titanium Oligomer Formation towards High-Efficiency and Green Synthesis of Titanium Containing Molecular Sieves, *Angew. Chem., Int. Ed.*, 2021, **60**, 3443–3448.
38 J. Xing, D. Yuan, H. Liu, Y. Tong, Y. Xu and Z. Liu, Synthesis of TS-1 zeolites from a polymer containing titanium and silicon, *J. Mater. Chem. A*, 2021, **9**, 6205–6213.
39 M. Tamura, W. Chaikittisilp, T. Yokoi and T. Okubo, Incorporation process of Ti species into the framework of MFI type zeolite, *Microporous Mesoporous Mater.*, 2008, **112**, 202–210.
40 Q. Guo, Z. Feng, G. Li, F. Fan and C. Li, Finding the "Missing Components" during the Synthesis of TS-1 Zeolite by UV Resonance Raman Spectroscopy, *J. Phys. Chem. C*, 2013, **117**, 2844–2848.
41 Z. Shan, Z. Lu, L. Wang, C. Zhou, L. Ren, L. Zhang, X. Meng, S. Ma and F.-S. Xiao, Stable Bulky Particles Formed by TS-1 zeolite Nanocrystals in the presence of H_2O_2, *ChemCatChem*, 2010, **2**, 407–412.
42 T. Ge, Z. Hua, J. Lv, J. Zhou, H. Guo, J. Zhou and J. Shi, Hydrophilicity/hydrophobicity modulated synthesis of nanocrystalline and hierarchically structured TS-1 zeolites, *CrystEngComm*, 2017, **19**, 1370–1376.
43 W. Fan, R. G. Duan, T. Yokoi, P. Wu, Y. Kubota and T. Tatsumi, Synthesis, crystallization mechanism and catalytic properties of Ti-rich TS-1 free of extraframework Ti species, *J. Am. Chem. Soc.*, 2008, **130**, 10150–10164.
44 M. G. Clerici, G. Bellussi and U. Romano, Synthesis of Propylene Oxide from Propylene and Hydrogen Peroxide Catalyzed by Titanium Silicalite, *J. Catal.*, 1991, **129**, 159–167.
45 M. Signorile, V. Crocellà, A. Damin, B. Rossi, C. Lamberti, F. Bonino and S. Bordiga, Effect of Ti Speciation on Catalytic Peroformance of TS-1 in the Hydrogen Peroxide to Propylene Oxide Reaction, *J. Phys. Chem. C*, 2018, **122**, 9021–9034.
46 M. Zhang, S. Ren, Q. Guo and B. Shen, Synthesis of hierarchically porous zeolite TS-1 with small crystal size and its performance of 1-hexene epoxidation reaction, *Microporous Mesoporous Mater.*, 2021, **326**, 111395.
47 M. Liu, J. Li, X. Chen, J. Song, W. Wei, Y. Wen and X. Wang, Preparation of anatase-free hierarchical titanosilicalite-1 in favor of allyc chloride epoxidation, *Microporous Mesoporous Mater.*, 2021, **326**, 111388.
48 Y. Jiao, A. L. Adedigba, Q. He, P. Miedziak, G. Brett, N. F. Dummer, M. Perdjon, J. Liu and G. J. Hutchings, Inner-connection and open pore hierarchical TS-1 with controlled framework titanium for catalytic cyclohexene epoxidation, *Catal. Sci. Technol.*, 2018, **8**, 2211–2217.
49 Y. Zuo, M. Liu, T. Zhang, L. Hong, X. Guo, C. Song, Y. Chen, P. Zhu, C. Jaye and D. Fischer, Role of pentahedrally coordinated titanium in titanium silicalite-1 in propene epoxidation, *RSC Adv.*, 2015, **5**, 17897–17904.
50 W. Song, G. Xiong, H. Long, F. Jin, L. Liu and X. Wang, Effect of treatment with different bases on the catalytic properties of TS-1/SiO_2 extrudates in propylene epoxidation, *Microporous Mesoporous Mater.*, 2015, **212**, 48–55.

51 A. Esposito, M. Taramasso and C. Neri, *US Pat*, 4396783, 1983.
52 Y. Liu, C. Zhao, B. Sun, H. Zhu and W. Xu, Preparation and modification of Au/TS-1 catalyst in the direct epoxidation of propylene with H_2 and O_2, *Appl. Catal., A*, 2021, **624**, 118329.
53 X. Nie, X. Ji, Y. Chen, X. Guo and C. Song, Mechanistic investigation of propylene epoxidation with H_2O_2 over TS-1: Active site formation, intermediate identification, and oxigen transfer pathway, *Mol. Catal.*, 2017, **441**, 150–167.
54 D. H. Wells, A. M. Joshi, W. N. Delgass and K. T. Thomson, A quantum chemical study of comparison of various propylene epoxidation mechanism using H_2O_2 and TS-1 catalyst, *J. Phys. Chem. B*, 2006, **110**, 14627–14639.
55 J. Limtrakul, C. Inntam and T. N. Truong, Density funcitonal theory study of the ethylene epoxidation over Ti-substituted silicalite (TS-1), *J. Mol. Catal.*, 2004, **207**, 139–148.
56 Z. Wu, B. Wang, J. Shi, P. Rui, X. Xie, W. Liao and X. Shu, The silanization process or the hydrothermal synthesis of hierarchical titanium silicalite-1, *Microporous Mesoporous Mater.*, 2021, **327**, 111407.
57 H. Liu, Y. Wang, T. Ye, F. Wang, S. Ran, H. Xie, J. Liu, Y. Li, B. Li, Y. Liu, Y. Chai and L. Wang, Fully utilizing seeds solution for solvent-free synthesized nanosized TS-1 zeolites with efficient epoxidation of cholopropene, *J. Solid State Chem.*, 2022, **307**, 122844.
58 L. Zhang, X. Zhu, X. Wang and C. Shi, The synthesis of pure and uniform nanosized TS-1 crystals with a high titanium content and a high space-time yield, *Inorg. Chem. Front.*, 2021, **8**, 5260–5269.
59 Y. Liu, F. Wang, X. Zhang, Q. Zhang, Y. Zhai, G. Lv, M. Li and M. Li, One-step synthesis of anatase-free hollow titanium silicalite-1 by the solid-phase conversion method, *Microporous Mesoporous Mater.*, 2022, **331**, 111676.
60 M. Li, Y. Zhai, X. Zhang, F. Wang, G. Lv, A. Rosine, M. Li, Q. Zhang and Y. Liu, $(NH_4)_2SO_4$-assisted synthesis of thin-walled Ti-rich hollow titanium silicalite-1 zeolite for 1-hexene epoxidation, *Microporous Mesoporous Mater.*, 2022, **331**, 111655.
61 J. Su, G. Xiong, J. Zhou, W. Liu, D. Zhou, G. Wang, X. Wang and H. Guo, Amorphous Ti species in titanium silicalite-1: Structural features, chemical properties, and inactivation with sulfosalt, *J. Catal.*, 2012, **288**, 1–7.
62 R. Millini, E. Previde Massara, G. Perego and G. Bellussi, Framework Composition of Titanium Silicalite-1, *J. Catal.*, 1992, **137**, 497–503.
63 A. Tuel and Y. Ben Taârit, Influence of the nature of silicon and titanium alkoxides on the incorporation of titanium in TS-1, *Appl. Catal., A*, 1994, **110**, 137–151.
64 G. J. Hutchings, D. F. Lee and A. R. Minihan, Epoxidation of allyl alcohol to glycidol using titanium silicalite TS-1: effect of the method of preparation, *Catal. Lett.*, 1995, **33**, 369–385.
65 J. Blanchard, S. Barboux-Doeuff, J. Maquet and C. Sanchez, Investigation on hydrolysis-condensation reactions of titanium(IV) butoxide, *New J. Chem.*, 1995, **19**, 929–941.
66 J. Muhlebach, K. Muller and G. Schwarzenbach, The Peroxo Complexes of Titanium, *Inorg. Chem.*, 1970, **9**, 2381–2390.
67 R. G. Brereton, *Applied Chemometrics for Scientists*, Wiley, 2007.
68 G. Ricchiardi, A. Damin, S. Bordiga, C. Lamberti, G. Spanò, F. Rivetti and A. Zecchina, Vibrational Structure of Titanium Silicate Catalyst. A Spectroscopic and Theoretical Study, *J. Am. Chem. Soc.*, 2001, **123**, 11409–11419.
69 A. Damin, S. Bordiga, A. Zecchina and C. Lamberti, Reactivity of Ti(IV) sites in Ti-zeolites: An embedded cluster approach, *J. Chem. Phys.*, 2002, **117**, 226–237.
70 F. Bonino, A. Damin, G. Ricchiardi, M. Ricci, G. Spanò, R. D'Aloisio, A. Zecchina, C. Lamberti, C. Prestipino and S. Bordiga, Ti-Peroxo Species in the TS-1/H_2O_2/H_2O System, *J. Phys. Chem. B*, 2004, **108**, 3573–3583.
71 M. Signorile, A. Damin, F. Bonino, V. Crocellà, G. Ricchiardi, C. Lamberti and S. Bordiga, Computational Assessment of Relative Sites Stabilities and Site Specific Adsorptive Properties of Titanium Silicalite-1, *J. Phys. Chem. C*, 2018, **122**, 1612–1621.
72 Modde 13 Software; Umeå, Sweden, 2020, Available Online: **https://www.sartorius.com/en/products/process-analytical-technology/data-analytics-software/doe-software/modde?gclid=CjwKCAjwiuuRBhBvEiwAFXKaNM5XdB5p1oonkutonEjqk72uuSniQRNaZNqpIKZe3pQs0t2VRutWkRoCNvYQAvD_BwE** (accessed on 23 March 2022).
73 The R Project for Statistical Computing, **https://www.r-project.org/**, (accessed 23 February 2022).
74 Å. Rinnan, Pre-processing in vibrational spectroscopy - when, why and how, *Anal. Methods*, 2014, **6**, 7124–7129.
75 R. Ravishankar, C. Kirschhock, B. J. Schoeman, P. Vanoppen, P. J. Grobet, S. Storck, W. F. Maier, J. A. Martens, F. C. De Schryver and P. A. Jacobs, Physicochemical Characterization of Silicalite-1 Nanophase Material, *J. Phys. Chem. B*, 1998, **102**, 2633–2639.
76 M. Signorile, L. Braglia, V. Crocellà, P. Torelli, E. Groppo, G. Ricchiardi, S. Bordiga and F. Bonino, Titanium Defective Sites in TS-1: Structural Insights by Combining Spectroscopy and Simulation, *Angew. Chem., Int. Ed.*, 2020, **59**, 18145–18150.
77 F. G. Dwyer and E. E. Jenkins, *US Pat*, 3941872, 1976.
78 A. Corma, State of the art and future challenges of zeolite as catalysts, *J. Catal.*, 2003, **216**, 298–312.
79 S. Gontier and A. Tuel, Synthesis of titanium silicalite-1 using amorphous SiO_2 as silicon source, *Zeolites*, 1996, **16**, 184–195.